International Journal of Soft Computing 4 (5): 223-228, 2009
ISSN: 1816-9503

Texture Analysis of Bone CT Images for Classification and Characterization of Bone Quality

T. Kalpalatha Reddy and N. Kumaravel
College of Engineering/ECE, Anna University, Chennai, India

Abstract: Bone architecture is an important factor that determines bone strength in addition to bone mass. Texture analysis of the trabecular bone pattern on axial dental CT is being investigated as a potential means to characterize the bone quality. In this study, we examined the use of an artificial neural network and features from different scales of curvelet transform analysis to obtain a measure related to bone architecture and quality. Texture features are extracted from 220 image regions of jaw bone CT images (both male and female) using spatial gray level dependence method, run length, histogram and curvelet transform. By using the Neural Network Classifier, the classification of bone samples at different locations of the jawbone region is performed. First the combination of the features from run length and first order statistics achieved overall classification accuracy ≥69.23%. Features selected from the curvelet based cooccurrence matrix performed better with overall classification accuracy >80%. In order to increase the success rate the classification is done using the combination of curvelet statistical features, run length and curvelet cooccurence features as feature vector and using this, a mean success rate of 97.2% is obtained.

Key words: Dental CT, curvelet, neural networks, GLRL, haralick features, cooccurrence matrix

INTRODUCTION

The overall dental implant success rate is considered to be influenced by both the volume (quantity) and density (quality) of available bone for implant placement. Accurate analysis of the bone content and architecture would facilitate clinical decision making regarding patient selection, implant type and surface and the surgical technique used (Krug *et al*., 2005; Cendre *et al*., 2000). The distribution of the mineral content in three dimensions, connectivity of the trabeculae, trabecular spacing, micro structural characteristics and finally the loading of the skeleton are some of the factors determining the biomechanical properties of the bone (Krug *et al*., 2005; Cendre *et al*., 2000; Thomas *et al*., 1996). The micro architecture of opened celled cancellous bone in highly anisotropic and varies with age, medical condition and gender (Jakubas *et al*., 2003). Although, men and women may lose cancellous bone at similar rates, the micro structural natures of cancellous bone lose may be different between the sexes. Men lose cortical bone mass linearly with increasing age but the rate of decline may not be as rapid as that in women (Simina and Najarian, 2009; Hannan *et al*., 1992). There may, however, acceleration in the rate of cortical bone loss in the most elderly men (Jakubas *et al*., 2003; Eriksen *et al*., 1985; Simina and Najarian, 2009). The difference in the rate of cortical bone loss between the sexes is accentuated by the smaller differences in peak cortical bone mass present in early adulthood.

With aging, osteoblasts in both sexes appear to deposit less in resorptive cavities of normal bone, resulting in decreased trabecular bone mean wall thickness. With aging vertebral bone from normal women tends to demonstrate both trabecular thinning and loss of horizontal trabeculae, whereas that from men reveals only trabecular thinning (Hannan *et al*., 1992; Riggs *et al*., 1981; Eriksen *et al*., 1985; Arivazhagan and Ganesan, 2006).

Correct segmentation and classification of bone tissue is absolutely crucial for developing an automated decision making system that would assist detection and diagnosis of bone structural changes (Krug *et al*., 2005; Cendre *et al*., 2000; Thomas *et al*., 1996; Jakubas *et al*., 2003). A couple of challenges of bone tissue segmentation from dental CT are the large number of CT slices and differences in bone density. Bone tissue is of two types; cortical and cancellous. Cortical bone has high density and therefore appears bright and uniform in the CT image on the other hand, cancellous bone has a spongy texture and its overall gray level is extremely close to that of the surrounding muscle tissue. Bones tend to appear to have different position, sizes and shapes in the exams from different patients but also in different slices of

Corresponding Author: T. Kalpalatha Reddy, College of Engineering/ECE, Anna University, Chennai, India

the CT exam. There are several approaches in literature for CT image segmentation that attempt to address the typical challenges of CT segmentation.

Image segmentation: The segmentation process allowing the separation of bone trabeculae from the remainder of the image is a crucial point because of its influence on the determination of parameters, which are characteristics of bone architecture. The segmentation of these images has to cope with the difficulty of keeping in the binary image the highest possible number of trabeculae owing to the presence of both bright and dark trabeculae. Due to the effects of the resolution close to the trabeculae size and of the variations of BMD within the sample, a global threshold cannot be used on these images. When the image presents a regular pattern (macro texture), the methods used are called structural because they are based on the extraction of the pattern. If the image does not contain such a pattern (microstructure), statistical methods are used. Tomographic images of cancellous jaw bone belong to the latter category (Simina and Najarian, 2009; Fukunaga, 1990). Thus, taking the local neighborhood of a pixel into account method using an edge enhancement process was investigated.

Fast discrete curvelet transform: Texture classification has been an important research topic in image processing. Now a day's classification based on wavelet transform is being very popular. Wavelets are very effective in representing objects with isolated point singularities, but failed to represent line singularities (Simina and Najarian, 2009; Chen *et al*., 2005). Recently, ridgelet transform which deal effectively with line singularities in 2-D is introduced (Arivazhagan and Ganesan, 2006; Lucia and Semlar, 2007). But images often contain curves rather than straight lines. To overcome the weakness of ridgelets in higher dimensions, Candes *et al*. (2006), Ying (2005) and Donoho and Duncan (2000) proposed a new system of representations called curvelet transform which is designed to handle curve discontinuities well. Curvelet allows representing edges and other singularities along curves in a more efficient way when compared with other transform.

Here the idea is to partition the curves into collection of ridge fragments and then handle each fragment using the ridgelet transform. The digital curvelet transform provides near optimal reconstruction of twice-continuously differentiable (C^2) curves (Candes *et al*., 2006; Ying, 2005; Donoho and Duncan, 2000; Chen *et al*., 2005). It is declared that curvelets offer optimal sparseness for curve-punctuated smooth images, where the image is smooth with the exception of discontinuities along C^2 curves. In images with the large number of C^2 curves (i.e., an image with a great number of long edges), it would be advantageous to use the curvelet algorithm. Unlike wavelets, curvelets are localized not only in position (the spatial domain) and scale (the frequency domain), but also in orientation. The curvelet transform is numerically tight frames and a multistage pyramid with many directions and positions at each length scale and needle shaped element at fine scales (Candes *et al*., 2006). This localization provides the curvelet frame with surprising properties; it is an optimally sparse representation for singularities supported on C^2 curves in two dimensions.

The second generation Discrete Curvelet Transform (Fast DCT) takes as input a Cartesian Grid of the form (Candes *et al*., 2006) $f(n_1, n_2)$, $0 \le n1$, $n_2 < n$ and outputs a collection of coefficients:

$$C^D(j,l,k) = \Sigma_{n_1 n_2} f(n_1, n_2)\, \Phi^D_{j,l,k}(n_1, n_2) \qquad (1)$$

where, $\Phi^d_{j,l,k}(n_1, n_2)$ are digital wavelet transforms with j standing $j \ge 0$ for scale, l for orientation and $k = (k_1, k_2)$ for spatial location.

A wedge like frequency window $\tilde{U}_{j,l}(w)$ is defined by:

$$\begin{aligned} &\tilde{U}_{j,l}(w) = W_j(w)\; V_{j,l}(w), \\ &W_j(w) = \sqrt{\Phi^2_{j+1}(w) - \Phi^2_j(w)}, \\ &V_{j,l}(w) = V(2^{\lfloor \frac{j}{2} \rfloor} w_2 - a_l\, w_1 / w_1)) \end{aligned} \qquad (2)$$

Where:

- w, w_1, w_2 = Frequency values
- $W_j(w)$ = The radial window
- $V(w)$ = The angular window, they are both smooth, non negative, real valued and obey the admissibility conditions
- al = A center slope for lth wedge
- Φ = Defined as the product of low-pass one dimensional windows, i.e., $\Phi_j(w_1, w_2) = \Phi(2^{-j} w_1)$, $\Phi(2^{-j} w_2)$ the function Φ is smooth, obeys $0 \le \Phi \le 1$, is equal to 1on [-1, 1] and vanishes outside of [-2, 2]

Coarsest scale ($j = j_0$): The coarsest scale curvelets are isotropic and the only index for l is zero, which can be defined by their D.F Transform:

$$\begin{aligned} \Phi^D_{j0,0}\, x(w) = \tilde{U}_{j0,0}(w) \exp[-2\pi i \\ (k_1 w_1 / l_1, j_0 + k_2\, w_2 / l_2, j_0)] \\ (0 \le k_1 < l_1, j_0,\; 0 \le k_2 < l_2, j_0) \\ \sqrt{l_1, j_0\, l_2, j_0} \end{aligned} \qquad (3)$$

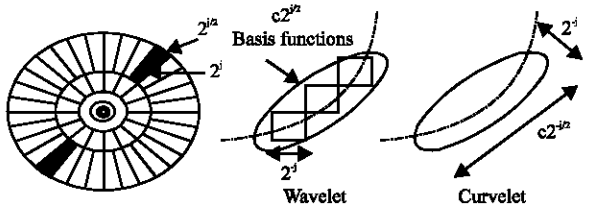

Fig. 1: Curvelet transform (Candes *et al*., 2006)

Fine scale ($j_0<j<j_e$): Coarsest each has poor quadrants: East, North, West and South, each Quadrants separated into $2^{j/2}$ wedges with the same areas (Fig. 1).

The discrete wavelet with index k at scale j and angle l is defined by means of its Fourier Transform:

$$\Phi^{D}_{j,k,l}(w) = \tilde{U}_{j,i}(w)\exp[-2\pi i (k_1 w_1/l_{1,j,i} + k_2 w_2/l_{2,j,i})] \quad (0 \le k_1 < l_{1,j,i},\ 0 \le k_2 < l_{2,j,i}) \quad \sqrt{l_1, j_0\ l_2, j_0} \tag{4}$$

Last scale $j = j_e \le \log 2\ (n/2)$: This final scale extracts the highest frequency content. The curvelets at this level are defined by:

$$\Phi^{D}_{je,0,l}(w) = \tilde{U}_{je,0}(w)\exp[-2\pi i (k_1 w_1/l_{1,je} + k_2 w_2/l_{2,je})] \quad (l_{1,j0} = l_{2,j0} = n, 0 \le k_1, k_2 < n) \quad \sqrt{l_1, j_e\ l_2, j_e} \tag{5}$$

Then, the curvelet coefficients can be defined as:

$$C(j,l,k) = C_0(0,0,k) + \Sigma_{j=1}^{je-1} C_F(j,l,k) + C_L(j_e,0,k) \tag{6}$$

Curvelets provides almost orthogonal decomposition with respect to basis functions that have far superior (e.g., Fourier, Radon, Wavelet) localization and sparseness properties than other transform. In Fig. 1, describes the curvelet partitioning of the frequency wave number plane. One wavelet lives in a wedge and becomes more directional selective and anisotropic for the higher frequencies (while moving away from the origin). Curvelets are localized in both the space (x, t) and spatial (KF)-domains and have, as consequence of their partitioning, the tendency to align themselves with curves/wave fronts.

MATERIALS AND METHODS

Texture analysis method: Since, texture analysis has been a topic of study since the early seventies, various feature extraction and classification techniques were proposed. They can be categorized into four major methods: statistical methods (co-occurrence method) (Arivazhagan and Ganesan, 2006; Haralick *et al*., 1973), geometrical (Voroni tessellation features) (Unser, 1986) and model based method (Markov random fields) (Yongqing and Yingling, 2006; Lucia and Semlar, 2007) and signal processing methods (Gabor filters, wavelet transform and curvelets) (Lucia and Semlar, 2007; Arivazhagan and Ganesan, 2006; Candes *et al*., 2006). The first step in texture analysis is the identification of proper features that maximize the differentiation of the textures for segmentation, classification and recognition. An image segmentation algorithm is either a pixel based or a region-based approach. In a region based approach, the image has to be segmented into homogeneous regions and a set of meaningful features has to be defined. Once defined, image regions (blocks) can be categorized using pattern recognition techniques. Features are assumed to be uniform with in regions of interest in the same texture. Haralick *et al*. (1973) proposed texture analysis based on first/second order statistics and co-occurrence matrix features. However, they generated 14 features for different distances at different orientations, which ultimately increased the computational and time complexity. Their maximum correct classification rate was only between 60-70%.

Feature extraction: Texture classification involves two phases' i.e., learning and classification. In the learning phase the original bone image is decomposed using Discrete Curvelet Transform (DCvT). Features such as mean and standard deviation are calculated from each of these curvelet sub-bands and are stored in the data base. Co-occurrence matrix (C) is formed for each sub-band of discrete curvelet transform, which gives the information about the spatial distribution of gray scale values. From the Co-occurrence matrix, the features such as contrast, sum-mean, cluster shade cluster prominence and local homogeneity are calculated (Haralick *et al*., 1973). From the run length matrices we have selected five features that presented a significant correlation with the mechanical response of bone (Fukunaga, 1990). Feature vector V1 contains 1st order gray level run length and histogram features such as mean, variance, kurtosis, long run emphasis, run percentage, gray level no uniformity and skewness. Feature vector V2 contains the features extracted from curvelet based cooccurance matrix, such as contrast, cluster shade, cluster prominence and local homogeneity and are stored in the database. In order to improve the classification gain the combination of feature vectors V1 and V2 are used as feature vector V3.

Classification: Another crucial component in texture analysis is the classifier being used. With years of study, this area has also produced a number of classifiers, such as: Nearest Neighbor, Fisher Linear Discriminate, Neural Networks, LVQ and Bayes classifier. Neural networks have been a natural choice as trainable pattern classifiers because of their capability to approximate functions and to generalize (Fukunaga, 1990). Artificial Neural Networks (ANN) are powerful computational systems consisting of many simple processing elements connected together to perform tasks analogously to biological brains. They are massively parallel, which makes them efficient, robust, fault tolerant and noise independent. They can learn from training data and generalize them to new situations. The learning process of the ANN is similar to the learning function of the brain. During training, samples are presented to the input layer that yields changes of the activation state of output processing elements (Fukunaga 1990). The calculated output value is compared to the required value which is also given in the training set. Depending upon the difference between the required and calculated output values, the network adjusts synaptic weights whose distribution constitutes the basis of the problem-solving algorithm. For the present study 90 (40 Male, 50 Female) patients were considered. The age, pathology and race were identified before the test. The performance of the neural networks was estimated using False Positive (FP), False Negative (FN), True Positive (TP) and True Negative (TN) values (Fukunaga 1990; Kornel *et al*., 1998). Classification of a normal data as abnormal is considered as FP and classification of abnormal data as normal is considered FN. TP and TN are the cases where the abnormal is classified as abnormal and normal classified as normal, respectively. The accuracy, sensitivity, specificity and adjusted accuracy were estimated using the following relation:

Accuracy	=	(TP+TN)/(TP+FP+TN+FN)
Sensitivity	=	TP/(TP+FN)
Specificity	=	TN/(TN+FP)
False positive rate	=	FP/(TN + FP)
Positive predictive value	=	TP/(TP + FP)
Negative predictive value	=	TN/(TN + FN)
Adjusted accuracy	=	(sensitivity + specificity)/2

Accuracy is the representation of classifier performance in global sense. Sensitivity and Specificity are the proportions of abnormal data classified as abnormal, normal data classified as normal respectively. The adjusted accuracy is a measure that accounts for unbalanced sample data of normal and abnormal events. The adjusted accuracy combines sensitivity and specificity into a single measurable value (Kornel *et al*., 1998; Fukunaga, 1990).

RESULTS AND DISCUSSION

A total of 90 patients participated in the study (40 male, 50 female and age range 30-65, mean age 50 years). Single, partial, or total edentulous patients were included. For all the patients, spiral CT was performed (GE medical systems) at 120 KV, 80 mA and 0.65 mm slice thickness. The 3D DICOM image data consists of 190 consecutive 2D slices, each slice being 512×512 pixels in size and having 16 bit gray level resolution. Gray level Threshold methods may not be sufficient for bone segmentation in CT due to varying bone density. Hence segmentation method based on edge tracing is used by choosing initial seeds by thresholding located fairly close to the desired edge. Figure 2 shows the original axial CT slice and segmented part of the bone image using region based and edge based segmentation. Curvelets like wavelets are extremely sensitive to contrast in the gray level intensity, the segmented images need further processing. In order to effectively use curvelet based texture descriptors, it is necessary to eliminate all background pixels to avoid mistaking the edge between the artificial background and the tissue as a texture feature. Each slice was therefore further cropped and only square 32×32 sub- image fully contained in the interior of the segmented area are generated. This size was chosen since the digital curvelet requires a 2^n square image (Candes *et al*., 2006). For our images of 32×32, maximum resolution extraction was three levels of resolution and 16 angles were found to be ideal. Figure 3 represents the curvelet decomposition of the segmented image at level 3. Several features were then calculated on the curvelet coefficients.

Classification of bone quality in different locations of jaw is done using three different feature vectors (V1-V3). Feature vector V1 contains the curvelet statistical features and gray level features such as energy entropy, GLNU, RLNU extracted from the sub image and curvelet sub-bands. Feature vector V2 contains curvelet co occurrence features such as contrast, cluster shade, local homogeneity etc calculated from the curvelet sub-bands. In order to improve the classification gain the combination of feature vectors V1 and V2 is used as feature vector V3. For the purpose of comparison, the result obtained using feature vector V3 is compared with V4 which contains the combination of Wavelet Statistical Features (WSF) and wavelet co-occurrence features (Reddy and Kumaravel, 2009).

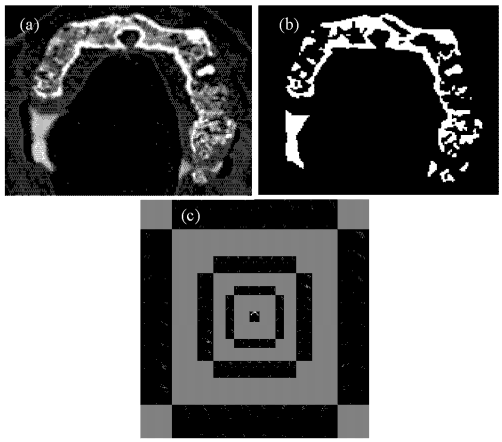

Fig. 2: a) Original axial CT slice, b) Edge based segmented image, c) Region based segmentation

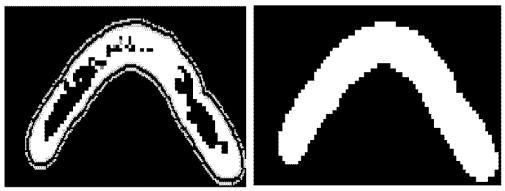

Fig. 3: Curvelet decomposition

The classification results obtained for three different feature vectors (V1-V3) using BPN network are given in Table 1, where each entry specifies the average classification efficiency (%) obtained.

Table 1 shows a comparison of the performance for three feature vectors. The results indicate that a combination of CSF+CCF are the most effective descriptors for curvelets.Feature vector V3 outperformed all other feature vectors having accuracy rates between 75-97%, which was higher than both V1(in the 33-67%) and V2 (between 60-75%). Table 2 shows the performance of the back propagation for different network topologies. The network has been tested with 10, 15 and 20 hidden layer neurons. Feature vector V3 with twenty hidden layer neurons outperformed all other feature vectors (with 10 and 15 hidden layer neurons) with accuracy rates between 84-97%. From the analysis of bone texture classification using curvelet transform, it is inferred that the mean success rate achieved shows good improvement i.e., 30% improvement over the mean success rate achieved using wavelet transform for the same data set (Reddy and Kumaravel, 2009). The improvement in success rate is due to the sparse representation of images using the curvelet transform where the most significant co-efficient represent the most energetic directions of an image with straight edges. Also ridgelet transform handles the co-efficient with all possible directions. So the images which contain curves can handle well using the curvelet transform. As a result, the features obtained from the curvelet sub bands will have powerful information compared to the features from the wavelet sub bands.

Table 1: Classification performance using back propagation network

		Classification efficiency			
Location	Bone images	V1	V2	V3	V4
Male	Anterior Maxilla (%)	33.33	60	81	33.33
	Posterior Maxilla (%)	50	62.5	90	60
Female	Anterior Maxilla (%)	66.66	67.5	75	56
	Posterior Maxilla (%)	57	75	94	87.5
Number of image regions correctly classified		115	145	200	135
Mean success rate (%)		52	66.25	90	60

V1 = CSFs; V2 = CCFs; V3 = CSFs+CCFs; V4 = WSFs + WCFs

Table 2: Classification performance using BPN with different network topology for anterior maxilla of female

Feature vector	Network topology	No. of training iterations	Classification performance (%)
V1	16-10-2	100	66.66
	16-15-2	200	84.61
	16-20-2	300	92.30
V2	12-10-2	100	66.53
	12-15-2	200	84.61
	12-20-2	300	75.92
V3	28-10-2	100	75.53
	28-15-2	200	83.92
	28-20-2	300	97.20

ACKNOWLEDGEMENTS

The researchers would like to thank Mr. Padmanabhan, Bharat Scans and Dr. B. Sarathi for their help in clinical data collection.

REFERENCES

Arivazhagan, S. and L. Ganesan, 2006. Texture classification using wavelet transform. Pattern Recogn. Lett., 27 (16): 1875-1883. DOI: 10.1016/J. patrec.2006.04.013.

Candes, E.J., L. Demanet, D.L. Donoho and L. Ying, 2006. Fast discrete curvelet transforms. Multistage Modeling and Simulation, 5 (3): 861-899. DOI: 10. 1137/05064182X. http://dx.doi.org.

Cendre, E., V. Kaftandjian, G. Preix, M. Joulin, D. Mitton and D. Babot, 2000. An investigation of segmentation methods and texture analysis applied to Tomographic images of human vertebral cancellous bone. J. Microscopy, 197 (3): 305-316 (12). DOI-10.1046/3. 1365-2818.2000.00670.X.

Chen, G.Y., T.D. Bui and A. Krzyak, 2005. Rotation invariant pattern recognition using ridgelet, wavelet cycle-spinning and Fourier features. Pattern Recognition, 38 (12): 2314-2322. DOI: 10.1016/J. patcog.2005.02-008.

Donoho, D.L. and M.R. Duncan, 2000. Digital Curvelet Transforms strategy, implementation and experiments. In: Proceedings of Aero Sense Wavelet Applications VII, Vol. 4056. SPIE, pp: 12-29. ID: 34999.

Eriksen, E.F., L. Mosekilde and F. Melsen, 1985. Trabecular bone resorption depth decreases with age: Differences between normal males and females. J. Bone, 6 (3): 141-146. DOI: 10.1016/8756-3282(85) 90046-8.

Fukunaga, K., 1990. Introduction to Statistical Pattern Recognition. 2nd Edn. Academic Press, San DiegoCA, USA. ISBN: 0-12-269851-7. www.academi-cpress.com.

Hannan, M.T., D.T. Felsen and J.A. Anderson, 1992. Bone mineral density in elderly men and women: Results from the Framingham osteoporosis study. J. Bone and Mineral Res., 7: 547-553. PMID: 1615761.

Haralick, R.M., K. Shanmugam and I. Dinstein, 1973. Texture features for image classification. IEEE. Trans. Syst., Man and Cybernetics, 8 (6): 610-621. DOI: 10. 1109/JSMC.1973.4309314.

Jakubas, J.P., A. Sawicki and P. Przecolocki, 2003. Assessment of trabecular bone structure in post menopausal and sensile osteoporosis in women by image analysis. Scand. J. Rheumatol., 32: 295-299. DOI: 10.1080/03009740310003938.

Kornel, P., M. Bela, S. Rainer, D. Zalan, T. Zsolt and F. Janos, 1998. Application of neural network in medicine. Diag. Med. Technol., 4 (3): 538-546.

Krug, R., J. Carballido-Gamito, A. Burgwardt, S. Haase, J.W. Sedat, W.C. Moss and S. Majumdar, 2005. Wavelet based characterization of vertebral trabecular bone structure from MR images of specimen at 3 tesla compared to micro CT measurements. Proceedings of the IEEE Engineering in Medicine and Biology 27th Annual Conference, Shangai, China, Sep. 1-4, pp: 7040-7043. DOI: 10.1109/ IEMBS.2005.1616127. INSPEC: 9208957.

Lucia, D. and L. Semlar, 2007. A comparison of wavelet, ridgelet and curvelet-based texture classification algorithms in computed tomography. Comput. Biol. Med., 37: 486-498. PubID: 17054933.

Reddy, T.K. and N. Kumaravel, 2009. Assessment of bone architecture using wavelet based multiresolution texture analysis. NCISE.

Riggs, B.L., H.W. Wahner, W.L. Dunn, R.B. Mazyess, K.P. Oherd and J. Melton, 1981. Differential changes in bone mineral density of the appendicular and axial skeleton with aging. The J. Clin. Investigation, 67 (2): 328-335. DOI: 10.1172/JCI110039. PMCID: PMC370572.

Simina, V. and K. Najarian, 2009. A unified method based on wavelet filtering and Active contour models for segmentation of pelvic CT images. Complex Medical Engineering, ICME International Conference, pp: 1-5. ISBN: 978-1-4244-3315-5. DOI: 10.1109/ICCME.2009. 4906670. INSPEC: 10615828.

Thomas, E. Southard and Kavin A. Southard, 1996. Detection of simulated osteoporosis in maxillae using radiographic texture analysis. IEEE. Trans. Biomed. Eng., 43 (2): 123-132. DOI: 10.109/10.481981. INSPEC: 5215006.

Unser, M., 1986. Local linear transform for texture measurements. Signal Process., 11: 61-79. DOI: 10. 1016/0165-1684(86)90095-2.

Ying, L., 2005. CurvelLab 2.0. California Institute of Technology.

Yongqing, X. and V.R. Yingling, 2006. Comparative assessment of bone mass and structure using texture-based and histomorphometric analysis. J. Bone, 40: 544-552. DOI: 10.1016/J.bone.2006.08.015. PII: S8756-3282(06)00688-0.